Large Eddy Simulation of Kerosene/LOx Supercritical Combustion Characteristics of a Swirl Injector using Steady Flamelet Model

Jun-Young Heo, Jeong-Seok Kang *, and Hong-Gye Sung**
**Korea Aerospace University*
Goyang Gyeonggi, 412-791, South Korea

Abstract

The turbulent mixing and combustion of a kerosene/liquid oxygen coaxial swirl injector under supercritical pressures has been numerically investigated. JP10 is employed for the kerosene thermodynamic properties. Turbulent numerical model is based on Large Eddy Simulation with real-fluid transport and thermodynamics over the entire pressure range; RK-PR Equation of State, Chung's model for viscosity/conductivity, and Fuller's theorem for diffusivity to take account Takahashi's compressible effect. A combustion model is applied to the real-fluid steady flamelet model which is based on kerosene/oxygen flame structure results. A comparison of swirl effect is investigated in order to investigate mixing and combustion dynamics inside an injector and a combustion chamber. It was revealed that combustion efficiency depends on the mixing rate according to the swirl intensity.

Nomenclature

D	=	Diffusivity
E	=	Specific total energy
f	=	Mixture fraction
p	=	Pressure
q	=	Heat flux
t	=	Time
u	=	Velocity components
x	=	Spatial coordinate
Z	=	Pseudo-time variable vector

Greek

δ	=	Kronecker delta
Γ	=	Preconditioning matrix or circulation
ρ	=	Density
τ	=	Viscous stress tensor

Superscripts

$\bar{}$	=	Resolved-scale
$\tilde{}$	=	Favre-averaged resolved-scale
$_{sgs}$	=	Subgrid-scale

1. Introduction

A liquid rocket engine for the space launch vehicle is operating at high pressure in order to increase the thrust and combustion efficiency so that its propellants are exposed to supercritical conditions in the combustion chamber. The supercritical condition is the state of the arbitrary substance being enclosed by the environment beyond its critical point. In such conditions, the propellants experience the transition of thermophysical properties differently than during this from regime change process at subcritical conditions. After the liquid propellant is introduced into the injector and combustion chamber, its properties are varied continuously and the distinction between gas and liquid is ambiguous. At supercritical conditions, the engine performance can be achieved with high energy density because propellant properties exhibit gas-like diffusivities and liquid-like densities. Also, their surface tension and enthalpy of vaporization reach zero. These phenomena affect the mixing and combustion dynamics sensitively. Because of the peculiarities of substances at supercritical conditions, the conventional methods for property analysis are inappropriate. Hence, the study of the mixing and combustion process of the propellants at supercritical conditions is an essential subject.

For understanding of the atomization, mixing, and combustion phenomena in advanced liquid rocket engines, experimental and numerical studies are performed in the wide range of pressure and temperature including the supercritical conditions. In research of numerical analysis, the mixing and combustion processes in shear coaxial injectors using propellants as methane/liquid oxygen and hydrogen/liquid oxygen at supercritical conditions have been investigated. The thermophysical characteristics of hydrogen and liquid oxygen flame in a shear coaxial injector at supercritical pressure have been investigated by Oefelein using direct numerical simulation [1]. Zong and Yang applied the large eddy simulation for the identification of cryogenic fluid dynamics in a swirl oxidizer injector operating at supercritical pressure [2]. Giorgi and Leuzzi performed the numerical analysis of mixing and combustion in methane and liquid oxygen shear coaxial injector at supercritical conditions [3]. Recently, Giorgi et al. simulated combustion characteristics of methane and liquid oxygen and compared between the results in accordance with combustion models, reaction mechanisms [4], and equations of state at supercritical conditions. Sierra et al. numerically investigated reaction mechanisms and combustion characteristics for the recess number using hydrogen and liquid oxygen as propellants [5]. Hiroshi et al. analysed nitrogen injection characteristics and compared between the numerical results to pressure and temperature in combustor [6]. H. Huo et al. simulated combustion characteristics in a kerosene and liquid oxygen supercritical injector applying the flamelet library technique as a combustion model [7].

In this study, on the basis of previous study [8, 9], the combustion of a kerosene and liquid oxygen coaxial swirl injector under supercritical pressures has been numerically investigated. Turbulent numerical model is based on LES with RK-PR equation of state [10], Chung's model [11] for viscosity/conductivity, and Fuller's theorem [12] for diffusivity to take account Takahashi's compressible effect. The effect of swirl intensity and pressure fluctuations are analyzed.

2. Numerical Method

2.1 Filtered Transport Equations

The theoretical formulation is based on the filtered Favre averaged mass, momentum, energy, and mixture fraction conservation equations in Cartesian coordinates. Turbulent closure is achieved by means of a LES technique in which large scale turbulent structures are directly computed and the unresolved small scale structures are treated by using the analytic or empirical modeling. The governing equations can be written as:

$$\frac{\partial \bar{\rho}}{\partial t} + \frac{\partial \bar{\rho}\tilde{u}_j}{\partial x_j} = 0 \tag{1}$$

$$\frac{\partial \bar{\rho}\tilde{u}_i}{\partial t} + \frac{\partial (\bar{\rho}\tilde{u}_i\tilde{u}_j + \bar{p}\delta_{ij})}{\partial x_j} = \frac{\partial (\bar{\tau}_{ij} - \tau_{ij}^{sgs} + D_{ij}^{sgs})}{\partial x_j} \tag{2}$$

$$\frac{\partial \bar{\rho}\tilde{E}}{\partial t} + \frac{\partial \left[(\bar{\rho}\tilde{E} + \bar{p})\tilde{u}_i \right]}{\partial x_i} = \frac{\partial}{\partial x_i}\left(\bar{q}_i + \tilde{u}_j\bar{\tau}_{ij} - Q_i^{sgs} - H_i^{sgs} + \sigma_{ij}^{sgs} \right) \tag{3}$$

$$\frac{\partial \bar{\rho}\tilde{f}}{\partial t}+\frac{\partial(\bar{\rho}\tilde{u}_i\tilde{f})}{\partial x_i}=\frac{\partial}{\partial x_i}\left(\bar{\rho}\tilde{D}\frac{\partial \tilde{f}}{\partial x_i}+\Phi_i^{sgs}\right) \quad \textbf{(4)}$$

The unclosed sub-grid scale terms are defined

$$\tau_{ij}^{sgs}=\bar{\rho}\left(u_iu_j-\tilde{u}_i\tilde{u}_j\right) \quad \textbf{(5)}$$

$$D_{ij}^{sgs}=\left(\bar{\tau}_{ij}-\tilde{\tau}_{ij}\right) \quad \textbf{(6)}$$

$$Q_i^{sgs}=\left(\bar{q}_{ij}-\tilde{q}_{ij}\right) \quad \textbf{(7)}$$

$$H_i^{sgs}=\bar{\rho}\left(Eu_i-E\tilde{u}_i\right)+\left(\overline{pu}_i-\bar{p}\tilde{u}_i\right) \quad \textbf{(8)}$$

$$\sigma_i^{sgs}=\left(\overline{u_j\tau_{ij}}-\tilde{u}_j\tilde{\tau}_{ij}\right) \quad \textbf{(9)}$$

$$\Phi_i^{sgs}=\bar{\rho}\left(u_if-\tilde{u}_i\tilde{f}\right) \quad \textbf{(10)}$$

τ_{ij}^{sgs}, D_{ij}^{sgs}, Q_{ij}^{sgs}, H_{ij}^{sgs}, σ_{ij}^{sgs} and Φ_{ij}^{sgs} are the sgs stress, nonlinearity of viscous stress term, heat flux, energy flux, viscous work, and conserved scalar flux, respectively. The dynamic Smagorinsky model is employed to close those sgs terms [13].

2.2 General-Fluid Thermodynamics and Transport

Intermolecular forces and the molecular body volume are considered as important factors in the real-fluid. In order to understand the real-fluid phenomenon, effects such as compressibility, van der Waals force, molecular dissociation, and non-equilibrium thermodynamic quantity must be taken into account. An equation of state capable of handling dynamics of real-fluid at high pressure and low temperature regime is required for thermophysical property evaluation of real-fluid. The RK-PR equation of state is adopted to calculate real-gas fluid properties because it is more accurate to predict the properties of kerosene and oxygen than the SRK, PR equation of state [9, 14].

RK-PR equation of state:

$$p=\frac{\rho R_uT}{\left(M_w-b\rho\right)}-\frac{a\alpha\rho^2}{\left(M_w+\delta_1b\rho\right)\left(M_w+\delta_2b\rho\right)} \quad \textbf{(13)}$$

2.3 Numerical Scheme

The governing equations are numerically solved by means of a finite volume method. This method allows for the treatment of arbitrary geometry. The spatial discretization employs a fourth order central differencing scheme in generalized coordinates. The temporal discretization is obtained by second order backward differencing scheme using a fourth order Runge-Kutta scheme for integration of the real time term. In the regions of low Mach number flows, the energy and momentum equations are practically decoupled and the system of conservation equations becomes stiff. Pressure decomposition and preconditioning techniques with dual time stepping are applied to circumvent the round-off errors associated with the calculation of the pressure gradient and the convergence difficulties for the low Mach number flows in the momentum equation. First, a rescaled pressure term is used in the momentum equation to circumvent the singular behavior of pressure at low Mach numbers. Second, a preconditioning technique with dual time-stepping integration procedure is established. A unified treatment of general fluid thermodynamics is incorporated into a preconditioning scheme. The pseudo-time derivative may be chosen to optimize the convergence of the inner iterations through the use of an appropriate preconditioning matrix that is tuned to rescale the eigenvalues to render the same order of magnitude to maximize convergence. To unify the

conserved flux variables, a pseudo-time derivative of the form $\Gamma \partial Z / \partial \tau$ can be added to the conservation equation. Since the pseudo-time derivative term disappears as the solution is converged, a certain amount of liberty can be taken in choosing the variable, Z. We take advantage of this by introducing a pressure p' as the pseudo-time derivative term in the continuity equation. The code is paralleled using an MPI library for more effective calculation.

3. Model Description

Figure 1 shows a coaxial swirl injector geometry and the swirl numbers of liquid oxygen and kerosene are 1.598 and 6.548, respectively. The injector includes three major parts: a tangential inlet, a vortex chamber, and a discharge nozzle. The kerosene (outer) and liquid oxygen (inner) injects into the swirl injector through the tangential passage. In case of quasi-3D simulation, the radial and azimuthal velocities are determined from the tangential inlet port angle and these velocity components are factor to set the swirl strength and mass flow rate, respectively.

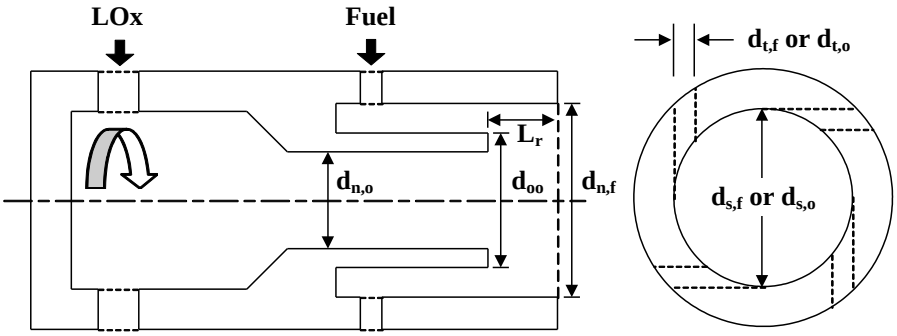

$$S_o = \frac{4 d_{s,o} d_{n,o}}{\pi n_{n,o} d_{t,o}^{\ 2}} = 1.598 , \quad S_f = \frac{4\left(d_{n,f} - d_{o,o}\right) d_{s,f}}{\pi n_f d_{t,f}^{\ 2}} = 6.548$$

Figure 1: Injector geometry and swirl number

Table 1: Operation conditions

Injector		Coaxial Swirl
Chamber Pressure		100 bar
Fuel		Kerosene; 350 K
Oxidizer		Liquid Oxygen; 103 K
Injector Pressure Drop	Fuel	9.5 bar
	Oxidizer	9.5 bar

Table 2: Computation conditions

Case	Equation of State	Dimension	Tangential Velocity
1	RK-PR	Quasi-3D	x1
2		Quasi-3D	x2

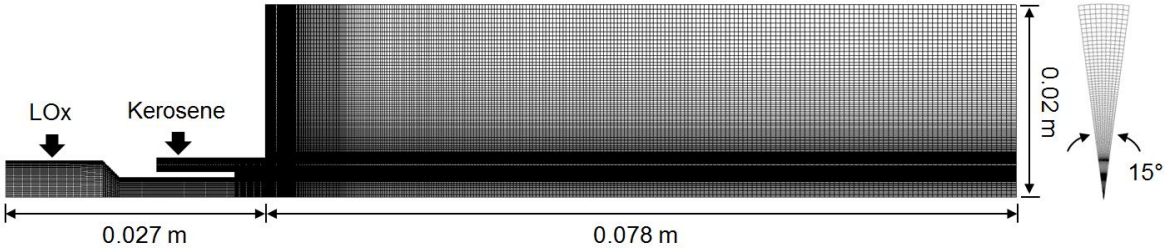

Figure 2: Computational domain (Quasi-3D)

Operation and computation conditions are listed in Table 1 and 2, respectively. Quasi-3D flow fields with periodic boundaries is treated herein because of the enormous computational time for simulating of full 3D using the large eddy simulation. The tangential inlets which are circular ports connected to the injector are approximated with a thin slit. Figure 2 shows a computational domain divided into 45 blocks, with each calculated on a single processor of a distributed computing facility. The total grid points are about 765 000 nodes. The disturbances at all of calculation conditions are generated by a Gaussian random-number generator with an intensity of 5% of the mean quantity.

4. Results and Discussion

4.1 Flame Structure

The surrogate model developed by San Diego Lab is employed for kerosene. The surrogate model is JP-10 which is consisted of one component (C10H16). Their detailed chemistry is composed of 263 reactions and 53 species. To solve the chemical kinetics, a FlameMaster code [15] is used in this study. The RK-PR model is applied to FlameMaster in order to consider the real-gas thermodynamic properties at supercritical conditions.

The flamelet library should cover an overall range of scalar dissipation rate, from chemistry equilibrium to extinction point. In this study, the flamelet library is generated that it considers to four scalar dissipation rates in range 2 (stable) to 950,000 (extinction) s-1. As the scalar dissipation rate increases, the flame becomes unstable and then extinction at scalar dissipation rate of 950,000. To reduce the computational load, nine species are selected for major components. For all points, the pressure is fixed as 100 bar, and the inlet temperatures of the fuel and oxygen take the corresponding the operating condition of the swirl injector. Figure 3 represents the species distribution at scalar dissipation rate of 1.3 which is near to the chemistry equilibrium. The Mass fractions and the gradient of mass fractions and mixture fractions for all species are determined by the filtered mixture fraction, mixture fraction variance, and the scalar dissipation rate from LES simulation.

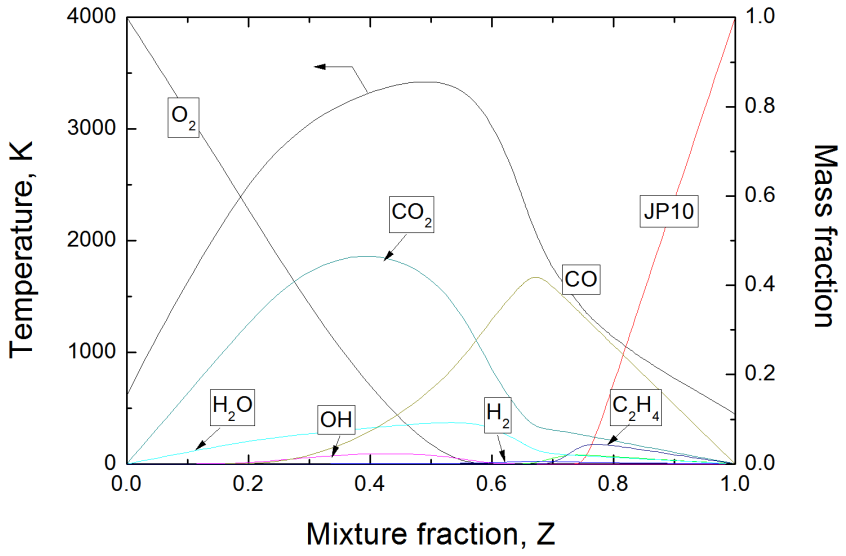

Figure 3: Temperature and mass fractions according to mixture fraction; 100 bar, χ=1.3

Figure 4 shows the maximum temperature distribution as a function of scalar dissipation rate and at various pressures. x-axis is log scale and y-axis is linear scale. Scalar dissipation rate controls the mixing of non-premixed combustion, since it controls the gradients of Z (mixture fraction). Also, different scalar dissipation levels lead to different flame structure [16]. Scalar dissipation rate provides the connection between the mixing field and the combustion modeling. In Fig. 4, at the fixed pressure, the maximum temperature remains constant for relatively small scalar dissipation rate and temperature decreases relatively larger rate until the extinction point is reached. Then, as the scalar dissipation rate decreases, the temperature keeps decreasing. And at the fixed scalar dissipation rate, as the pressure increases, the maximum temperature increases, because the dissociation which makes the flame temperature lower is restrained by high pressure. The extinction scalar dissipation rate increases as the pressure increases. This means that high pressure operating condition is more resistant to no equilibrium state. Figure 5 shows

the extinction scalar dissipation rate as a function of pressure. As the pressure increases, scalar dissipation rate almost grows linearly with pressure.

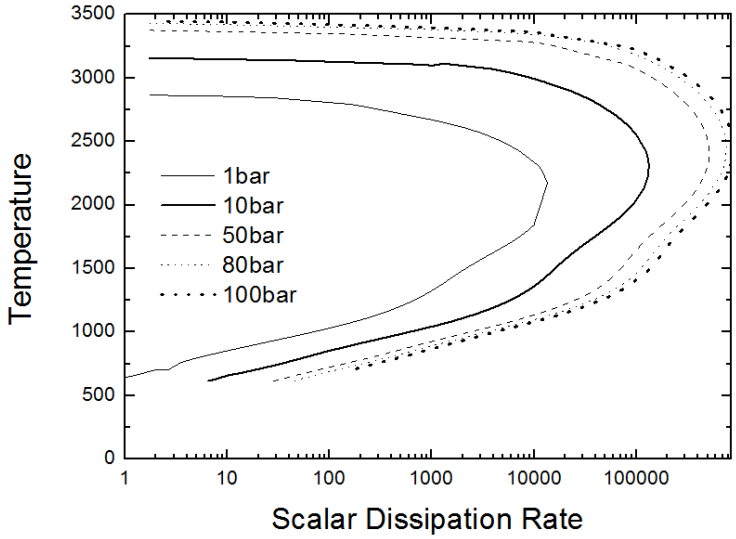

Figure 4: S-curve at various scalar dissipation rate and pressure

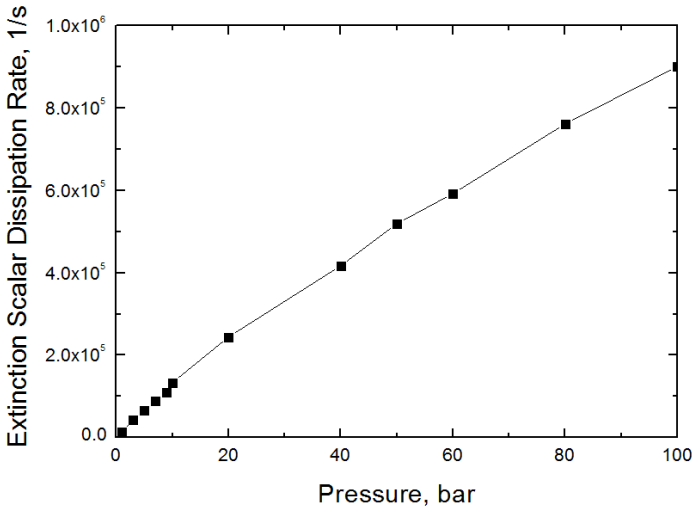

Figure 5: Extinction Scalar Dissipation Rate to Pressure

4.2 Swirl Intensity Effect

Two tangential velocities are applied to investigate the swirl strength effect on combustion characteristics. Figure 6 represents the temperature fields for each swirl strength. The formed liquid oxygen film is closer to the injector wall since a centrifugal force of swirl flow becomes stronger as the tangential velocity increases. As the swirl strength is stronger, the gas phase core is formed in the central region of oxidizer injector which affects the film boundary area enlarged in the injector and facilitates vorticity breakup. In both cases, the flame in the region close to the splitter is stabilized. Fresh oxidizer and fuel are brought into the mixing layer. As the parings of vortices involve larger scales of mixing, the flame rapidly spreads outward and forms intensive burning regions. As the flames are generated at the tip and convected downstream, multiple pairings of vortices grow up gradually. The flame may shed off from the main flame structure, when mixing with cold reactants, losing energy to them due to heat transfer. The flame generally continues to follow the shape of the oxygen jet and is very close to the high density oxygen. This tendency occurs because the stoichiometric mixture fraction is 0.2329 for JP10/Oxygen.

To quantify the level of performance of injectors, combustion efficiency is considered using the following formula:

$$\eta(x) = \frac{\int \rho Y_{Fuel} u \alpha dA}{\int \rho Y_{Fuel} u dA} \qquad \alpha = \begin{cases} 1 & (\phi_{local} \le \phi_{global}) \\ \dfrac{1}{\phi_{local} / \phi_{global}} & (\phi_{local} > \phi_{global}) \end{cases} \tag{14}$$

Where ρ and Y_{Fuel} are density and mass fraction of kerosene, respectively. The u is the velocity component normal to the area, dA, ϕ_{local} and ϕ_{global} are local and global equivalence ratio, respectively. The parameter α is decided by local equivalence ratio. This parameter means that if the local equivalence ratio is equal or less than global equivalence ratio, the mixing is regarded as completed. On the other hand, local efficiency is less than 1 when local equivalence ratio is large. Therefore, the combustion efficiency represents how much fuel spread into combustion chamber, in other words, the efficiency becomes 1 when local equivalence ratio is equal to global equivalence ratio through whole cross sectional area.

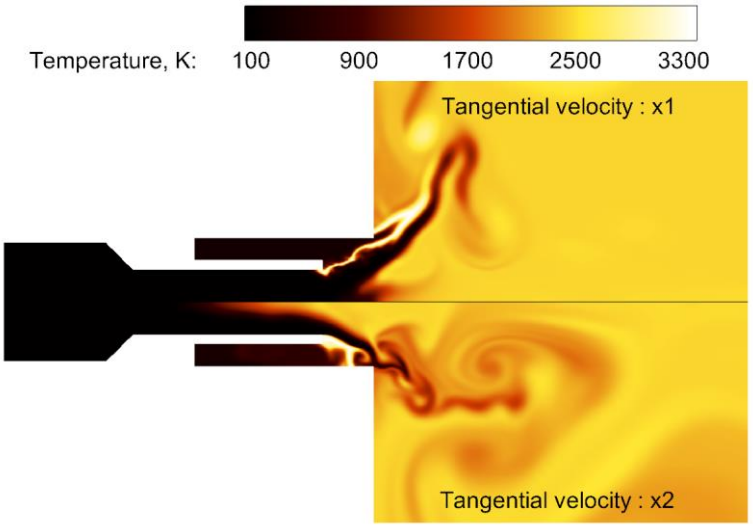

Figure 6: Instantaneous temperature contour according to swirl intensity

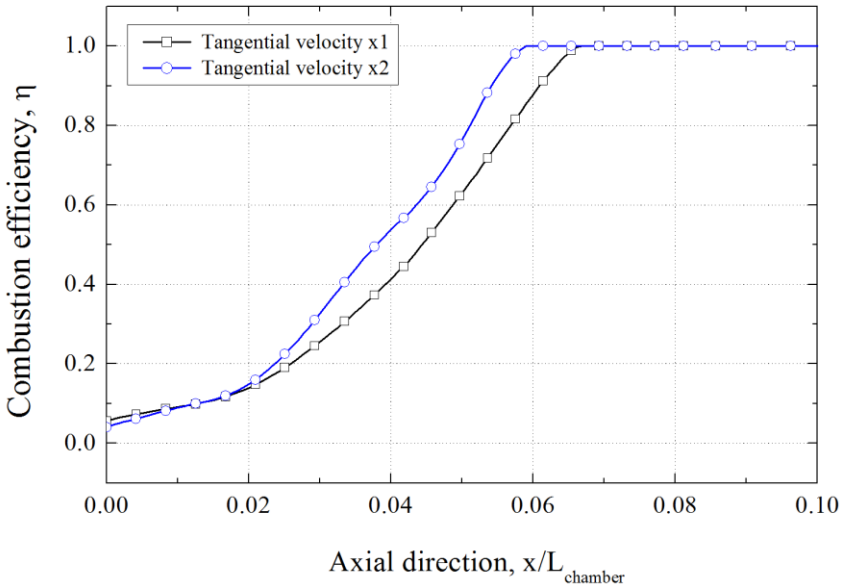

Figure 7: Combustion efficiency at different swirl intensity

Figure 7 shows combustion efficiencies on the time averaged fields. The efficiency increases as moves to downstream after the oxidizer injector post where the flame generates. Earlier, the combustion efficiency reached 1.0 when the tangential velocity increases to 2 times. Due to the swirl intensity to be strong, the spray angle of the liquid oxygen increases and the film forms inside the oxidizer injector with the strong swirl flow resulting in the rapid mixing of fuel and oxidizer.

Figure 8 represents the instantaneous distributions of temperature, mixture fraction, mass fractions of JP10, O_2, OH, and scalar dissipation rate. The flame anchors at the end of LOx post tip and spreads to combustion chamber with swirl angle. The flame is attached at the LOx post because the scalar dissipation rate which is calculated by simulation is smaller than a value of the extinction condition in library. Liquid oxygen is mixed with kerosene so that the diffusion flame in proper mixing ratio of the O/F is kept constantly in the recirculation zone. Because of the strong turbulence and thermal diffusion, the mixing between fuel and oxygen is more active and leads to generate a brighter flame in the injector backward. These strong flames are surrounding the spray cone of the liquid oxygen. The pressure wave generated in combustor interact with the liquid film of the oxygen, it promotes the gasification of the oxygen. Furthermore, this feature makes that the liquid film becomes dynamic and unstable, and affects the flame structures after injector. The feedback effects are very important to evaluate the dynamic characteristics in the combustion chamber. The species mass fraction contours as well as the temperature show that there is unburned liquid oxygen generating the central toroidal recirculation zone due to the swirl flow. And the unburned oxygen continues to mix with kerosene in the combustor, resulting secondary flame structures. Secondary flames were also observed in Singla et al.'s experimental- and Huo's numerical study [17, 18]. In this study, the secondary flames are formed from large-scale mixing and insufficient small-scale mixing of fuel and oxidizer as well as Huo's study, which is different from those observed in Singla‘s experiments, where droplets penetration through the flame accounts for the secondary flame. The flame structure correlates strongly with the mixing layers because the flame is controlled by diffusion- and mixing mechanism. As shown in JP10 mass fraction snapshot, the rapid thermodynamics variations are observed in the direction of steep density gradients since the combustion process causes to very large temperature gradients.

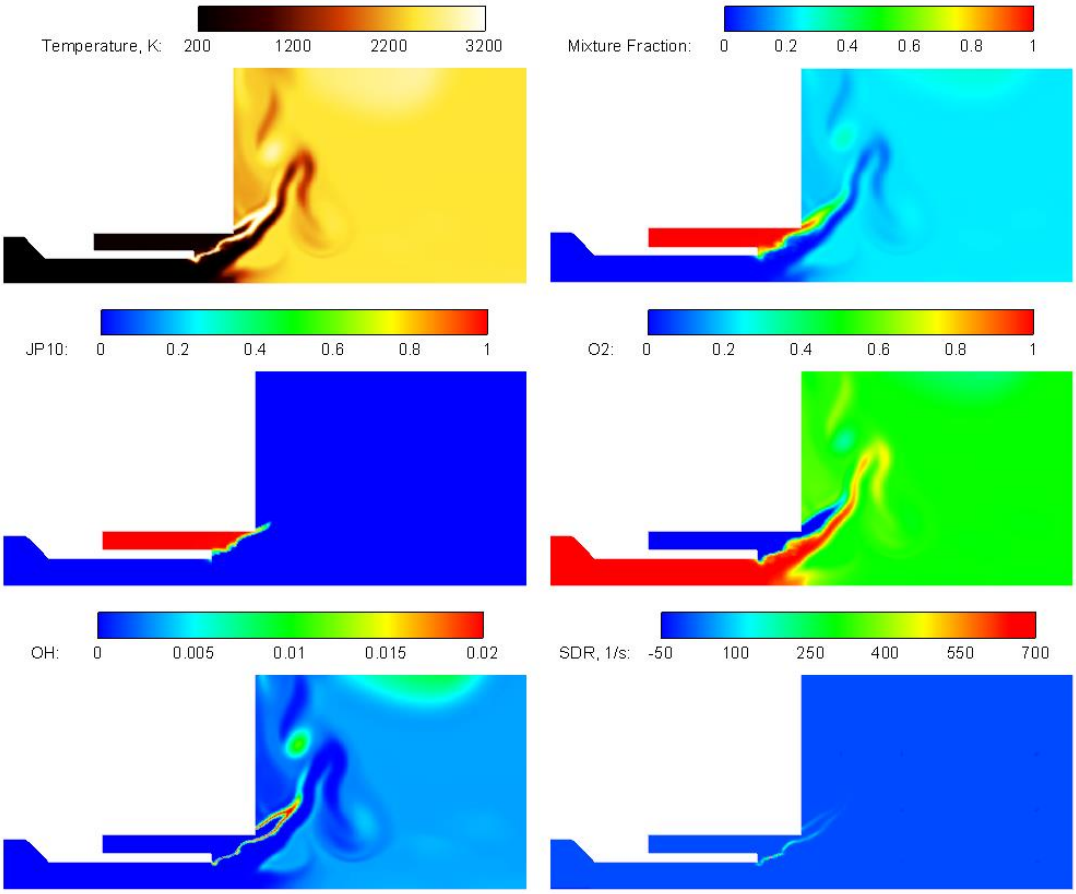

Figure 8: Instantaneous snapshots for tangential velocity x1 case

5. Conclusions

The combustion characteristics of co-axial swirl injector are investigated according to swirl intensity under supercritical condition. The RK-PR equation of state is adopted to calculate real-gas fluid properties because it is more accurate than the SRK, PR equation of state. A combustion model is applied to the real-fluid steady flamelet model. The reaction mechanism which is developed by San Diego Lab is calculated and the result is used to generate a flamelet library. The surrogate model is JP-10 which is consisted of one component (C10H16). Their detailed chemistry is composed of 263 reactions and 53 species. To solve the chemical kinetics at supercritical conditions, a modified FlameMaster code is used in this study. In order to compare the combustion efficiency according to the swirl intensity, inlet conditions are controlled by different tangential velocities. As the swirl intensity increases, the efficiency reaches 1.0 more quickly and the gaseous core is obviously formed inside oxidizer injector. Also, gasification of the liquid oxygen is facilitated from the core boundary. It was means that combustion efficiency depends on the mixing rate according to the swirl intensity.

Acknowledgement

This work was supported by Advanced Research Center Program (NRF-2013R1A5A1073861) through the National Research Foundation of Korea(NRF) grant funded by the Korea government(MSIP) contracted through Advanced Space Propulsion Research Center at Seoul National University. This research was partially supported by National Space Laboratory (NSL) Program (No. 2008-2006287) through the National Research Foundation of Korea (NRF) funded by the Ministry of Education, Science and Technology.

References

[1] Oefelein, J. C. 2005. Thermophysical Characteristics of Shear Coaxial LOx-H2 Flames at Supercritical Pressure. *Proceedings of the Combustion Institute*. Vol. 30. Issue 2. 2929-2937.

[2] Zong, N. and Yang, V. 2008. Cryogenic Fluid Dynamics of Pressure Swirl Injectors at Supercritical Conditions. *Physics of Fluids*. Vol. 20. Issue 5. 056103-1-14.

[3] Giorgi, M. G. D. and Leuzzi, A. 2009. CFD Simulation of Mixing and Combustion in LOx/CH4 Spray Under Supercritical Conditions. *39th AIAA Fluid Dynamics Conference*.

[4] De Giorgi, M., G., Sciolti, A., Ficarella, A. 2011. Comparisons between Different Combustion Models for High Pressure LOx/CH4 Jet Flame. *AIAA Fluid Dynamics Conference and Exhibit*.

[5] Sierra, P., Masquelet, M., Menon, S. 2013. Large-Eddy Simulation of a Reactive Shear Coaxial Injector Configuration. *AIAA Aerospace Sciences Meeting*.

[6] Hiroshi, T., Mitsuo, K. 2013. Characterization of Cryogenic Nitrogen Jet Mixings under Supercritical Pressures. *AIAA Aerospace Sciences Meeting*.

[7] Huo, H., Yang, V. 2013. Large-Eddy Simulation of Supercritical Combustion of Liquid Oxygen and Kerosene of a Bi-Swirl Injector. *AIAA Aerospace Sciences Meeting*.

[8] Heo, J. Y., Kim, K. J., Sung, H. G. 2011. Numerical Study on Kerosene/LOx Supercritical Mixing Characteristics of a Swirl Injector. *AIAA Aerospace Sciences Meeting*.

[9] Heo, J. Y. 2015. Numerical Study on Supercritical Mixing and Combustion Characteristics of a Kerosene/LOx Co-axial Swirl Injector. *Ph.D. Thesis, Korea Aerospace University.*

[10] Cismondi, M. and Mollerup, J. 2005. Development and Application of a Three-Parameter RK-PR Equation of State. Fluid Phase Equilibria. Vol. 232. Issue 1-2. 74-89.

[11] Chung, T., Ajlan, M., Lee, L. L., Starling, K.E. 1988. Generalized multiparameter correlation for nonpolar and polar fluid transport properties. *Industrial & Engineering Chemistry Research*. Vol. 27. 671-679.

[12] Takahashi, S. 1974. Preparation of a generalized chart for the di_usion coe_cients of gases at high pressures. *Japanese J. of Chem. Eng*. Vol. 7. No. 6. 417-420.

[13] Lilly, D. K. 1992. A proposed modification of the Germano subgrid-scale closure method. *Physics of Fluids*. Vol. 4. 633-635.

[14] Kim, S. K., Choi, H. S., Kim, Y. M. 2012. Thermodynamic Modeling Based on a Generalized Cubic Equation of State for Kerosene/LOx Rocket Combustion. Combustion and Flame. Vol. 159. Issue 3. 1351-1365.

[15] Pitsch, H. 2006. A C++ computer program for 0D combustion and 1D laminar flame calculations. *http://www.stanford.edu/group/pitsch/FlameMaster.htm*.

[16] Poinsot, T., Veynante, D. Theoretical and Numerical Combustion 3rd edition, CNRS.

[17] Singla, G., Scouflaire, P., Rolon, C., and Candel, S. 2005. Transcritical Oxygen/Transcritical or Supercritical Methane Combustion. *Proceedings of the Combustion Institute*. Vol. 30. 2921-2928.

[18] Huo, H. 2011. Large-Eddy Simulation of Supercritical Fluid Flow and Combustion. *Ph.D. Thesis, The Pennsylvania State University.*